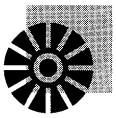

Contributed Paper

Characteristics of Post-Disruption Runaway Electrons with Impurity Pellet Injection

KAWANO Yasunori, NAKANO Tomohide, ISAYAMA Akihiko, ASAKURA Nobuyuki, TAMAI Hiroshi, KUBO Hirotaka, TAKENAGA Hidenobu, BAKHTIARI Mohammad, IDE Shunsuke, KONDOH Takashi and HATAE Takaki

Japan Atomic Energy Research Institute, Naka Fusion Research Establishment
801-1 Mukoyama, Naka, Ibaraki, 311-0193 Japan

(Received 26 November 2004 / Accepted 20 May 2005)

Characteristics of post-disruption runaway electrons with impurity pellet injection were investigated for the first time using the JT-60U tokamak device. A clear deposition of impurity neon ice pellets was observed in a post-disruption runaway plasma. The pellet ablation was attributed to the energy deposition of relativistic runaway electrons in the pellet. A high normalized electron density was stably obtained with $n_e^{bar}/n^{GW} \sim 2.2$. Effects of prompt exhaust of runaway electrons and reduction of runaway plasma current without large amplitude MHD activities were found. One possible explanation for the basic behavior of runaway plasma current is that it follows the balance of avalanche generation of runaway electrons and slowing down predicted by the Andersson-Helander model, including the combined effect of collisional pitch angle scattering and synchrotron radiation. Our results suggested that the impurity pellet injection reduced the energy of runaway electrons in a stepwise manner.

Keywords

tokamak, JT-60, disruption, runaway electrons, mitigation, impurity pellet, avalanche generation, slowing down, stopping power, synchrotron radiation

1. Introduction

Relativistic runaway electrons are generated in the tokamak device when electrons are continuously accelerated by an electric field to high energy that overcomes the deceleration drag mechanisms in a plasma [1]. In particular, many runaway electrons can be generated during a major disruption with an energy level of up to several tens MeV when sufficiently high toroidal electric field is induced [2]. As a result, runaway plasma in which most of the plasma current is driven by runaway electrons can be formed at the post-disruption phase.

In the International Thermonuclear Experimental Reactor (ITER), it is predicted that runaway electron current would reach a level of more than half that of the pre-disruption plasma current [2,3]. Runaway electrons generated by the disruption could damage first wall materials and in-vessel components of ITER. For instance, a numerical simulation study indicated that beryllium armor would be melted for a few millimeter thickness by localized deposition of 10 MeV runaway electrons with a power density of 50 MWm^{-2} [4]. Therefore, to establish ways to avoid the generation of runaway electrons is an important topic in ITER [1,5]. And in fact, several techniques have been demonstrated to avoid runaway electrons generation at disruption [6-11].

It is also important to mitigate the once generated runaway electrons at the post-disruption phase. A basic approach is to keep the runaway plasma in a divertor configuration to avoid unfavorable localized irradiation of runaway electrons to the first wall, and to await gradual reductions in the energy and population of runaway electrons [12]. These reductions can be stimulated by applying a negative loop voltage. However, such an approach is prevented by the fast growth of positional instabilities like the vertical displacement event (VDE) [13]. It is also prevented by a failure to achieve the desired position and shape control of the plasma. When VDE occurs, however, runway electrons are quickly exhausted from the plasma due to the spontaneous appearance of large-amplitude MHD activities when the plasma surface safety factor q_s becomes as small as 2 or 3 concomitant with a decrease in the plasma minor radius [14-16]. This is desirable from the viewpoint of terminating runaway electrons, but the pulsed and localized heat load on the first wall due to the irradiation of exhausted runaway electrons as in the study of H. Tamai et al. [15] becomes a concern.

Based on the background above, we have investigated an approach to mitigate and terminate runaway electrons by the use of external actuators, e.g., pellet injection. In a previous

author's e-mail: kawano@naka.jaeri.go.jp
This article is based on the invited talk at the 21st JSPF Annual Meeting (2004, Shizuoka).

study, hydrogen pellet injection into a discharge with runaway electrons during the flat top phase was carried out in the TEXTOR tokamak [17]. The discharge was terminated by the pellet injection with appearance of stochastic MHD activities in the bulk plasma. However, it is not clear whether a similar behavior occurs in a post-disruption runaway plasma in which most of the current is driven by runaway electrons and the bulk plasma temperature is as low as ~10 eV. Impurity pellet injection into RF current driven plasmas of the JIPP T-IIU tokamak has shown a pellet deposition profile different than that using Ohmic plasmas [18], and current-driven plasmas could survive against the impurity pellet injection, while Ohmic plasmas were disrupted. However, the conditions were different from those in the post-disruption runaway plasmas, since the temperature of the target bulk electrons was relatively as high as ~300 eV, and the temperature of the non-thermal tail electrons produced by RF current drive was non-relativistic and as low as 90 keV.

In this paper, the first experiment to study the effects of impurity pellet injection on post-disruption runaway electrons [19,20] is described. Newly revealed characteristics of a runaway plasma are also presented.

2. Evolution of Runaway Electrons and External Actuators for their Mitigation

The temporal evolution of runaway electrons is approximately expressed as [14]

$$dn_r/dt = n_e \nu_{coll} S(E/E_c^D, Z_{eff}) + n_r/\tau_s - n_r/\tau_{loss} , \quad (1)$$

where n_r is the density of runaway electrons, n_e the density of bulk plasma electrons, ν_{coll} the bulk electron collision frequency, Z_{eff} the effective charge of plasma, and E the electric field parallel to the magnetic field. The 1st term and the 2nd term on the right-hand side of eq. (1) indicate the generation of runaway electrons by the Dreicer process and the generation by the avalanche process, respectively. Here, the critical electric field of the Dreicer process, E_c^D, is expressed as

$$E_c^D = e^3 n_e Z_{eff} \ln\Lambda / (4\pi\varepsilon_0^2 m_e v_{th}^2) , \quad (2)$$

where e is the electron charge, m_e the electron rest mass, c the speed of light, ε_0 the dielectric constant of vacuum, $\ln\Lambda$ the Coulomb logarithm, and v_{th} the electron thermal velocity. This E_c^D provides the condition under which the most of thermal electrons run away. The critical electric field of the avalanche process E_c^A is written as

$$E_c^A = e^3 n_T \ln\Lambda / (4\pi\varepsilon_0^2 mc^2) \sim 0.12 \times 10^{-20} n_T , \quad (3)$$

where n_T is the total density of free and bound electrons in a plasma. In the avalanche process, new runaway electrons are generated by close collision with existing runaway electrons. The energy distribution of avalanche runaway electrons would have an exponentially folding shape. When $E > E_c^A$ and all newly generated avalanche runaway electrons are confined in a plasma, the time constant for the exponential growth of the number of runaway electrons τ_s is expressed as [21]

$$\tau_s = 2m_e c \ln\Lambda a(Z_{eff}) / eE , \quad (4)$$

where $a(Z_{eff}) = (2 + Z_{eff})/3$ [22]. Here, the toroidal electric field $E_t = V_{loop}/2\pi R_p$ supplies the accelerating electric field, where V_{loop} is the one turn loop voltage and R_p the plasma major radius. In large tokamak devices, it is recognized that the avalanche process could be the major process for generation of runaway electrons during a disruption due to their fast growth under a high electric field. For instance, in JT-60U, τ_s is calculated as ~70 ms for $E \sim E_t \sim 1.5$ V/m ($V_{loop} \sim 30$ V), ~7 ms for $E \sim E_t \sim 15$ V/m ($V_{loop} \sim 300$ V), in the case of $R_p = 3.3$ m, $\ln\Lambda = 18$, $Z_{eff} = 3$. The 3rd term on the right-hand side of eq. (1) is the time constant of the loss process τ_{loss}, which represents any loss and dumping process of runaway electrons.

At first, the slowing down of relativistic electrons by collisional friction with bulk plasma is considered to be a basic process for mitigation of runaway electrons. The friction force F_{fric}, which includes contributions from both bulk electrons and ions to relativistic electrons, is written by [23] as

$$F_{fric} = (e^4 n_e \ln\Lambda / 4\pi\varepsilon_0^2 m_e c^2)\{1 + (Z_{eff} + 1)/\gamma\} , \quad (5)$$

and then the frictional slowing down time τ_{fric} is defined as

$$\tau_{fric} = \gamma m_e c / F_{fric} , \quad (6)$$

where γ is the relativistic Lorentz factor defined as $\gamma = mc^2/m_e c^2 = (1 - \beta^2)^{-1/2}$, β the ratio of the speed of electron v to c defined as $\beta = v/c$, m the mass of a relativistic electron. In the high γ region, τ_{fric} becomes longer as γ increases, and it is noteworthy that F_{fric} has a weak dependence on γ and hence on Z_{eff}. In the case of $\gamma = 40$, which corresponds to energy of runaway electron W_r of ~20 MeV, and $Z_{eff} = 3$, $\tau_{fric} = 6.8 \times 10^{19} n_e^{-1}$; then $\tau_{fric} \sim 6.8$ s for $n_e = 1 \times 10^{19}$ m^{-3} and $\tau_{fric} \sim 0.68$ s for $n_e = 1 \times 10^{20}$ m^{-3}.

Candidates for external actuators include (i) injection of massive impurities or hydrogen to increase the friction force due to high n_e (and Z_{eff} in the case in impurities), (ii) plasma heating to modify bulk plasma parameters such as n_e, T_e, Z_{eff}, and E, (iii) applying a negative loop voltage to reduce the energy of runaway electrons and to avoid new generation by the avalanche process, and (iv) applying an error field for excitation of large-amplitude MHD activities. As the fist step, we consider that impurity pellet injection can be a good candidate as a quick actuator for increase in n_e and Z_{eff}. However, since the bulk electron temperature T_e is as low as ~10 eV for a post-disruption runaway plasma, as measured by Thomson scattering diagnostic in JT-60U [24], the ablation rate of a pellet by bulk electrons seems very small. So, we expect that the pellet ablation occurs due to runaway electrons themselves.

3. Experiment and Analysis

3.1 Formation of post-disruption runaway plasma

Figure 1 shows the schematic for the impurity pellet injection experiment into a post-disruption runaway plasma in JT-60U, and Fig.2 shows waveforms of the experiment (discharge number E38150). A series of impurity neon ice pellets (2.1 mm cube (~ 4×10^{20} neon atoms), ~700 m/s, 5 Hz, low field side mid-plane injection) are injected into an Ohmically heated hydrogen discharge with parameters of I_p = 0.85 MA, B_t = 3.73 T, a_p~1.1 m, R_p~3.5 m, V_p~85 m^3, q_s~13, $n_e(0)$~1×10^{19} m^{-3}, $T_e(0)$~2.3 keV, where I_p is the plasma current, B_t the toroidal magnetic field, a_p the averaged plasma minor radius, and V_p the plasma volume, and where "(0)" denotes the value at the plasma center. The 1st pellet functions as a "killer pellet" [6] to cause an intentional disruption accompanied by a runaway plasma phase with a starting current of ~0.5 MA. For the period of t = 12.24 s ~ 12.29 s, the central ECRF injection (O-mode, f_{ECRF} = 110 GHz, P_{ECRF}~500 kW) was applied to study its effects on the runaway plasma, but apparent responses were not observed. For t = 12.3 s ~ 13.15 s in Fig.2, V_{loop} is less than ~5 V. Since the Ohmic current for V_{loop} ~5 V is estimated to be as negligibly small as <10 kA due to the high plasma resistivity for low T_e of ~10 eV and Z_{eff}~3, most of the plasma current is driven by runaway electrons. Unfortunately, reliable T_e measurement for the runaway plasma was not available for this experiment. However, in cases in which a sufficient number of runaway electrons were not generated, we usually observed that the plasma vanished away even with similar or higher loop voltage at the disruption, and this fact supported the notion that the plasma current is mainly driven by runaway electrons. The plasma current ~0.5 MA corresponds to the total number of runaway electrons of $N_r = 2\pi R_p I_p/ec$~2.3×10^{17} electrons. In order to study the effects of impurity pellet injection, the current control of the runaway plasma was programmed for a stable target with a slightly decreased current, as indicated by the command value I_p^{com} in Fig.2. It is noteworthy that there were no large amplitude MHD activities at the impurity pellet injections during the runaway plasma phase, and thus the effects of MHD activities for mitigating runaway electrons would not seem to be particularly significant.

Figure 3 shows the changes in plasma shape and position. A divertor configuration was maintained until t~12.95 s, and then the plasma began to shrink with outer-touched limiter configuration. The analyses and discussions in the later sections were made mainly for the period in which the divertor configuration was maintained.

3.2 Deposition of impurity pellets in runaway plasma and evaluation of the charge number

Six successive neon ice pellets were injected into the post-disruption runaway plasma, and we observed a clear increase in the line-integrated bulk electron density, $\int n_e dl$, measured by far-infrared laser interferometry along the central vertical chord ch.2 (r/a~0) for the 2nd to 4th pellet injection,

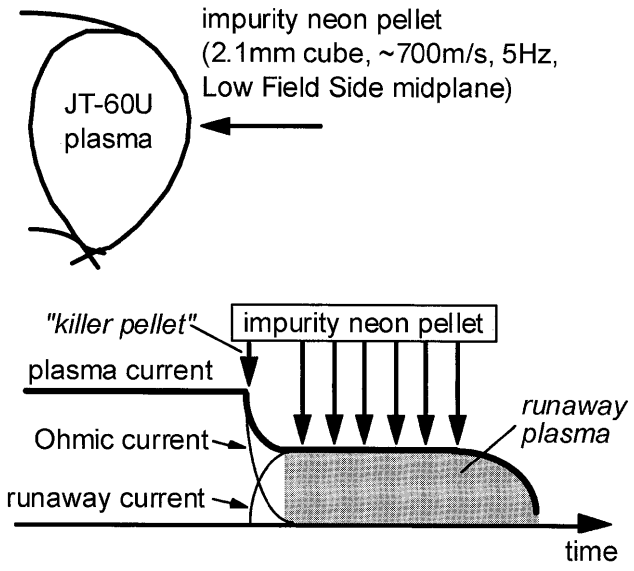

Fig. 1 Schematic of the experiment of impurity neon pellet injection in JT-60U to study mitigation effects on a post-disruption runaway electrons.

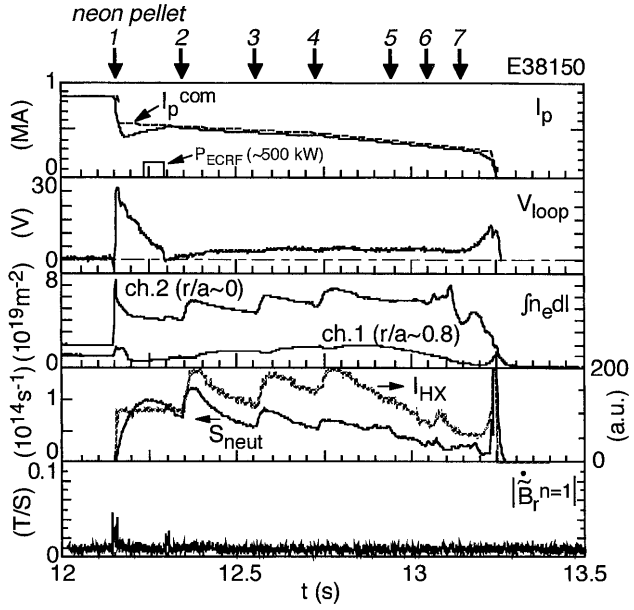

Fig. 2 Waveforms of the experiment of impurity neon pellet injection into the post-disruption runaway plasma (discharge number E38150). I_p: plasma current, I_p^{com}: command value of plasma current, P_{ECRF}: injection power of ECRF, V_{loop}: one turn loop voltage, $\int n_e dl$: line integrated electron density, S_{neut}: photo-neutron emission rate, I_{HX}: hard X-ray intensity (X-ray energy > ~1 MeV), $|\tilde{B}_r^{n=1}|$: amplitude of MHD activity of n = 1 mode.

as shown in Fig.2 ("a" is the plasma minor radius along radial direction). These increments of bulk electron density show that the impurity neon pellets were deposited in the post-disruption runaway plasma. However, as seen in Fig.2, the post-disruption runaway plasma survived and showed good resistance against these impurity pellet injections. Hence, the

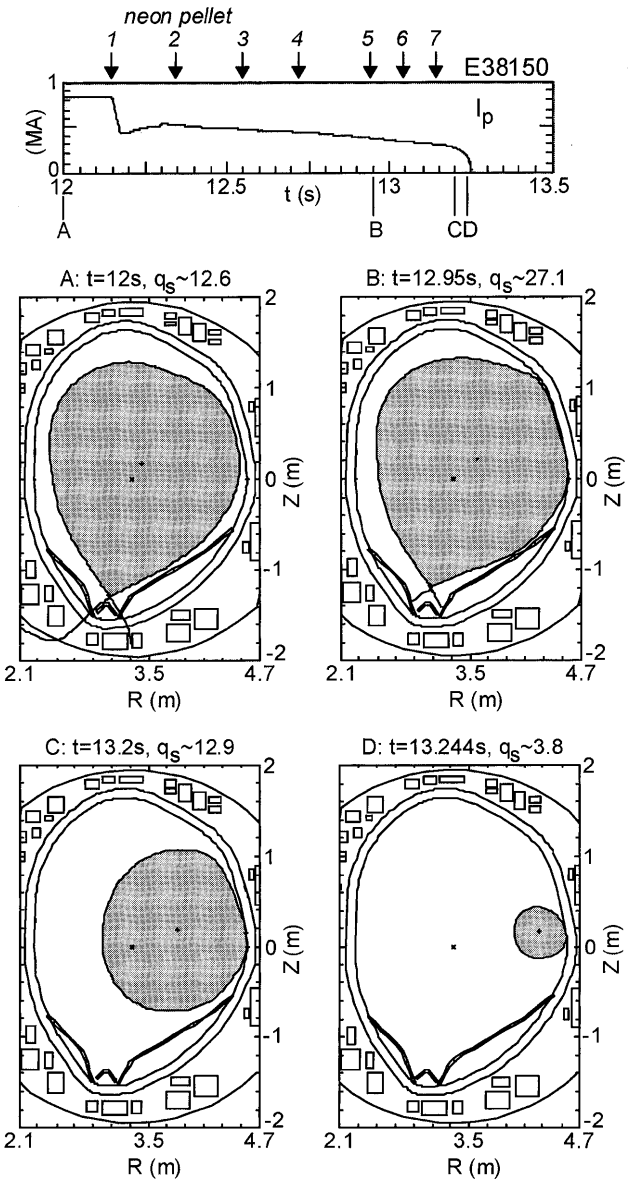

Fig. 3 Change in the plasma shape and position for the experiment of impurity neon pellet injection into the post-disruption runaway plasma. q_s: surface safety factor of plasma.

post-disruption runaway plasma exhibited different behavior than that of the standard Ohmic discharge.

The ablation rate for the neon ice pellet by the bulk electrons is given by the neutral gas shielding (NGS) model [25] as

$$dN_p/dt = k_z n_e^{0.333} T_e^{1.64} r_p^{1.333} M_i^{-0.333}, \quad n_e \text{ in cm}^{-3}, T_e \text{ in eV}, \tag{7}$$

where N_p is the number of ablated pellet atoms, k_z the coefficient for the pellet of the Z atom ($k_z = 2.32 \times 10^{15}$ s^{-1} for neon), r_p the pellet radius, and M_i the atomic mass in amu ($M_i = 20.18$ for neon). According to this model, the ablation rate and ablation time of the 1st pellet (killer pellet) can be estimated for different T_e as ~6.7×10^{22} atoms/s and ~6 ms for T_e = 1 keV, ~1.3×10^{23} atoms/s and ~3 ms for T_e = 1.5 keV, and ~2.6×10^{23} atoms/s and ~1.5 ms for T_e = 2.3 keV. Since these ablation times are comparable to the transverse time of the pellet in the plasma calculated as $2 \times a$/pellet speed ~2.2 m/(~700 m/s) ~ 3 ms, the 1st pellet seems to have been ablated well in the plasma. (This is supported by the rise time of $\int n_e dl$ (r/a~0) after the 1st pellet injection of ~5 ms.) On the other hand, the ablation times of the 2nd to 4th pellet in the runaway plasma are calculated as about 10 s for T_e~10 eV. Such a very long ablation time means that the pellet ablation by the bulk electrons was not effective.

Therefore, we conjecture that the runaway electrons made a significant contribution to the pellet ablation. Under the simple assumption that the spatial profile of runaway electrons is flat in the plasma, ~1.1×10^{16} runaway electrons would pass through a pellet cross section over a period of 3 ms. Taking the mass stopping power of a 20 MeV runaway electron due to the ionization process of neon as ~2 MeV/(g/cm^2) (see Fig.10), the mass density of solid neon as ~1.44 g/cm^3, and the target length as ~2 mm, the deposited energy to the pellet is calculated to be ~6.8×10^{15} MeV. (The contribution from the stopping power due to bremsstrahlung radiation ~0.7 MeV/(g/cm^2) is neglected here, since that radiation seems to pass through the pellet.) Then, with the average energy to create a neon ion of ~36.6 eV [26], ~1.9×10^{20} neon atoms can be ionized for 3 ms, and this number is about the half of the number of neon atoms in the pellet. (The sublimation energy of neon ice is as small as 0.022 eV/atom [25], and it is neglected here.) The runaway electrons presumably have a centrally peaked profile, which is supported by the visible TV camera images, and thus the number of ionized neon atoms seems to be increased by the increase in deposited energy. Though this is a very rough estimation and the change in pellet size during ablation process is not included, it seems reasonable to expect that nearly all or a substantial number of neon atoms in the pellet are ionized. In the experiment, rise times of increments of $\int n_e dl$(r/a~0) were observed as 30~50 ms. To explain these rise times, we consider a hypothesis that the ionization of neon is progressed by runway electrons (and/or by bulk electrons) up to the equilibrium ionization point that is mainly determined by T_e.

In the runaway plasma, the central bulk electron density was increased with each impurity pellet injection, as seen in $\int n_e dl(r/a$~0), while there were only slight responses in $\int n_e dl(r/a$~0.8). This means that the pellet was not deposited at the peripheral and edge region of r/a > ~0.8 but at the central region of the plasma. As a result, the profile of bulk electron density became peaked profile. Actually, at t~12.78 s in the discharge E38150 (see Fig.2), the ratio of $\int n_e dl(r/a$~0) to $\int n_e dl(r/a$~0.8) was ~4.8, while the ratio at t~12 s was ~2. At that time, the Greenwald density factor n_e^{bar}/n^{GW} became ~2.2, where n_e^{bar} ~2.9×10^{19} m^{-3}, $n^{GW} = I_p/\pi a^2$ ~1.3×10^{19} m^{-3}, I_p~0.42 MA, a ~1 m. It is also seen that this high bulk electron density was stably obtained. Thus, good particle confinement in the runaway plasma is indicated. When we consider that the ordinary density limit is dependent on the power balance

between the Ohmic input and radiation loss, and hence that the ordinary density limit is related to T_e, this high density would seem to be due to the fact that the runaway current is basically independent of the power balance.

It is important to know Z_{eff} and the charge number of neon Z_{Ne} of the runaway plasma for evaluation of the slowing down time of runaway electrons. The Z_{eff} value is evaluated from the visible bremsstrahlung emission measurement obtained in another discharge E38152 as shown in Fig.4. Since the intensity of visible bremsstrahlung emission I_{vb} is proportional to $\int Z_{eff} n_e^2 T_e^{-1/2} dl$, the ratio of I_{vb} to $(\int n_e dl)^2$, K, indicates $Z_{eff}^{bar}(T_e^{bar})^{-1/2}$ ("bar" denotes the line averaged value.) The value of Z_{eff}^{bar} before disruption at t~11.9 s is calculated to be ~1.3 using the profile data of n_e and T_e. The change in K between before the disruption phase (t = 12 s) and the runaway plasma phase (t = 12.5 s) is seen as ~20 in Fig.4. When we take T_e^{bar} of ~1 keV before the disruption phase and ~10 eV during the runaway plasma phase, the change in Z_{eff}^{bar} should be approximately twofold; hence Z_{eff}^{bar} during the runaway phase is estimated as ~2.6 in this discharge, and it does not vary substantially during this period. As shown in Fig.4, the ECRF injection and the helium gas puffing were applied in this discharge, but no significant responses were observed. For the discharge E38150, unfortunately I_{vb} was saturated at pellet injection timings due to higher detector sensitivity. However, based on a measured Z_{eff}^{bar} value of ~1.5 before disruption and assuming the same multiplication factor of ~2 obtained in E38152, Z_{eff}^{bar} is evaluated to be ~3 for the runaway plasma phase in E38150.

By looking at the response of the bulk electron density, we can also estimate Z_{Ne} of the plasma. For the 2nd pellet, the increment of the line-averaged electron density $\Delta\{\int n_e dl(r/a\sim0)/\int dl\}$ of ~0.72×10^{19} m^{-3} ($\int dl$ is the chord length of the interferometry in the plasma ~2.3 m) is ~30% of that for the 1st "killer pellet" of ~2.4×10^{19} m^{-3}. If we assume that the neon atoms are fully ionized for the 1st pellet, i.e., Z_{Ne} is 10, Z_{Ne} for the 2nd pellet can be estimated as ~3. Also, Z_{Ne}~3 is consistent with the expected ionization equilibrium of neon calculated for T_e = 10 eV.

These analyses first showed that the post-disruption runaway plasma with impurity neon pellet injections is nearly the neon plasma of $Z_{Ne} \sim Z_{eff}$ ~3 for T_e~10 eV and $n_e^{bar}/n^{GW} > \sim 2$.

3.3 Prompt exhaust of runaway electrons by impurity pellet injection

For injections of the 2nd to 4th pellets, an increase in the neutron emission rate S_{neut} was observed, as shown in Figs.2 and 5. The S_{neut} indicates the photo-neutrons emitted when high energy runaway electrons were exhausted from the plasma. In the case that runaway electrons hit the target structure, intense bremsstrahlung gamma rays can be produced, and these gamma rays can interact with the nuclei of the target materials via the photo-nuclear reaction, which in turn can cause photo-neutrons to be emitted from those nuclei. There are no measurements to show the distribution of hit points of runaway electrons, but the divertor tiles are a possible target, since the runaway electrons transported to the scrape-off layer

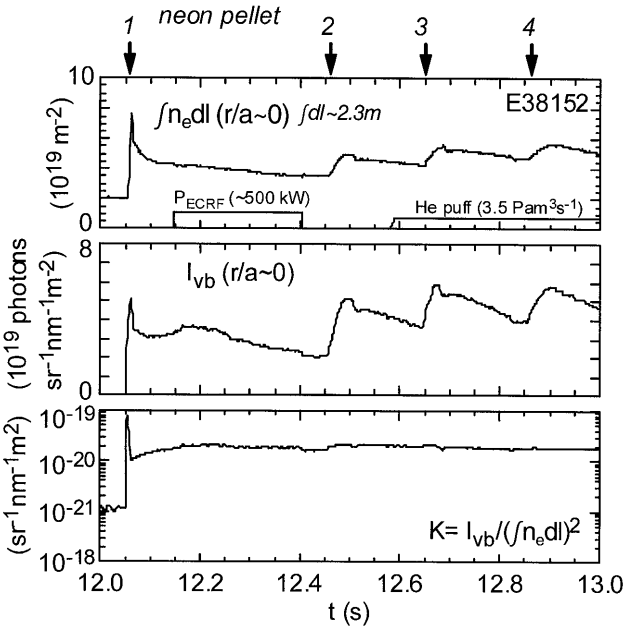

Fig. 4 Data from the visible bremsstralung emission measurement for evaluation of Z_{eff} (discharge number E38152). $\int n_e dl$: line integrated electron density, I_{vb}: intensity of visible bremsstralung emission, K: ratio of I_{vb} to $(\int n_e dl)^2$.

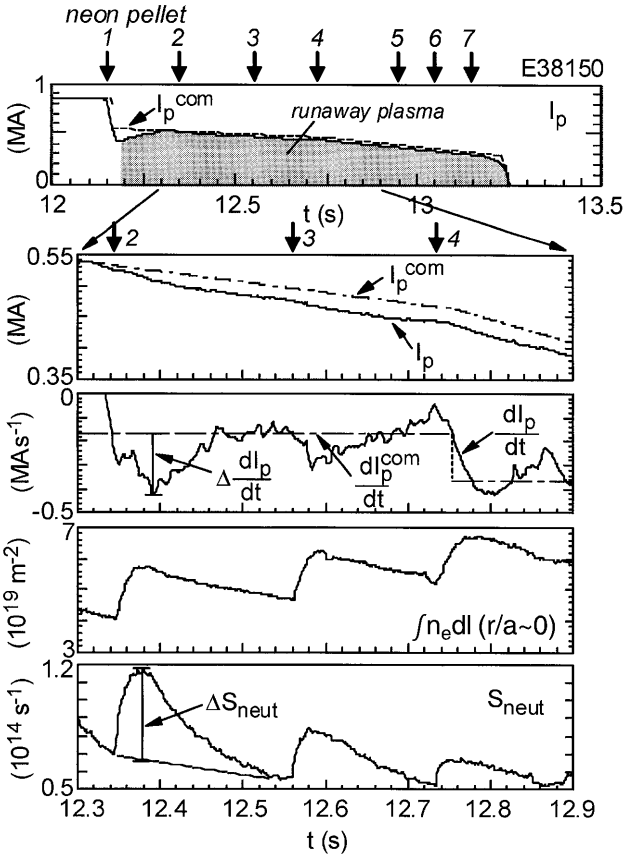

Fig. 5 A detailed waveforms of the experiment of impurity pellet injection into the post-disruption runaway plasma. dI_p/dt: decay rate of plasma current (with 10 ms signal filtering), dI_p^{com}/dt: command value of decay rate of plasma current.

may pass along the open magnetic field line. Another possible target is the outer board first wall for runaway electrons in the case that their drift orbit is shifted outward to approach the first wall. Therefore, one of the main elements for the photo-nuclear reaction is the carbon which is used for the divertor tiles and first wall tiles. Considering the penetration of gamma rays in the target material, another important element would be the nickel abundantly included in the Inconel 625 alloy which is used for the vacuum vessel. The threshold energies of photo-nuclear reactions are ~26 MeV for carbon and 8~30 MeV for nickel, respectively [27]. The free-fall accelerated electron energy is calculated with accelerating loop voltage (flux change) as $\gamma = [1 + \{e\int V_{loop}dt/(2\pi R_p m_e c)\}^2]^{1/2}$ [27] to be ~24 MeV with $\int V_{loop}dt$ ~1.7 Vs at t = 12.3 s. Though we should recognize that the energy distribution of runaway electrons must be spread, we consider that the maximum energy of runaway electrons W_r can be up to 20~30 MeV at t = 12.3 s.

By looking at the waveform of I_p corresponding to the increase in S_{neut} in detail, we observed a reduction of runaway plasma current, as seen in Fig.5. The current decay rate, dI_p/dt, clearly shows such a reduction apart from the command value dI_p^{com}/dt. After such a reduction, I_p recovers to approximately the command value again. We think this recovery is mainly due to the new generation of runaway electrons by the avalanche process, as discussed below in Sec. **3.4**.

For the period between t = 12.34 s and t = 12.39 s in Fig.5, the reduction of I_p is estimated as ~3 kA, which corresponds to a loss of ~1.5×10^{15} runaway electrons, and the increment of the neutron yield is ~1.5×10^{12} neutrons during the same period. Here, the ratio of neutron yield per runaway electron Y_n is approximately ~10^{-3}. A scaling law for determining the photo-neutron yield for disruption-generated runaway electrons was developed in JET as $Y_n = (W_r/60) \times 2.9 \times 10^{-3}$ neutrons per electron [27]. Then, when we take W_r = 20 MeV, a similar value of Y_n ~10^{-3} is obtained from the scaling law. This indicates that the exhaust of runaway electrons from the plasma makes a substantial contribution to the reduction of I_p. Since signals from two neutron monitors which are installed apart from each other in the toroidal direction show similar signals of photo-neutrons, we conclude that the runaway electrons were exhausted with good toroidal symmetry. The rise time of S_{neut} of 30~50 ms is longer than the time scale of S_{neut} observed in the termination by a large MHD burst during VDE as ~5 ms [15]; this seems to be a better condition from the viewpoint of reduction of the peak irradiation power onto target tiles. These are beneficial features for avoiding localized and pulsed irradiation of runaway electrons to the wall.

Figure 6 shows the relationship between the increment of the decay rate of the runaway plasma current $\Delta\tau_{Ip\text{-}decay}$ and the increment of the photo-neutron signal ΔS_{neut} for the 2nd to 4th pellet injections. Since there is an approximately linear relationship between $\Delta\tau_{Ip\text{-}decay}$ and ΔS_{neut}, the larger reduction of the runaway current is attributed to the larger exhaust of runaway electrons

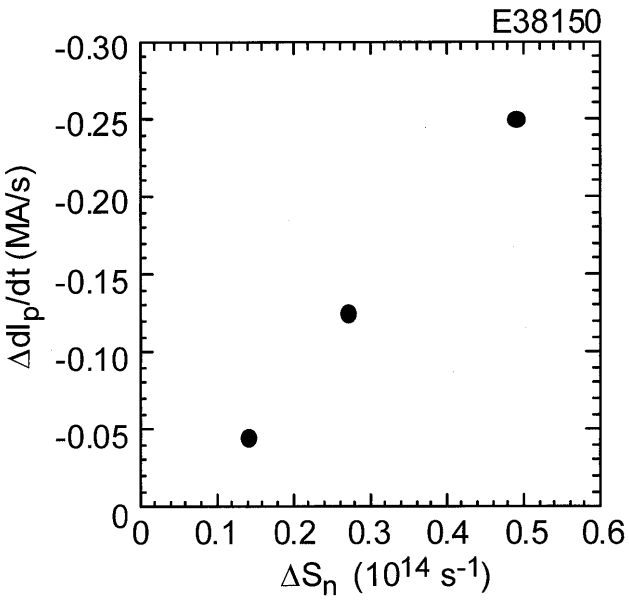

Fig. 6 Relationship between the increment of the decay rate of the runaway plasma current $\Delta dI_p/dt$ and the increment of the photo-neutron emission rate ΔS_{neut} for the 2nd to 4th pellets injection. Definitions of $\Delta dI_p/dt$ and ΔS_{neut} are shown in Fig.5.

3.4 Characteristic time scales for behavior of runaway plasma current

Figure 7 shows the behavior of characteristic time scales for the post-disruption runaway plasma current. The decay time of the runaway plasma current $\tau_{Ip\text{-}decay} = I_p/(-dI_p/dt)$ at the pellet interval time, e.g., t~12.55 s, is ~ 3 s, which is similar to the command value of the current decay time $\tau_{Ip\text{-}decay}{}^{com} = I_p{}^{com}/(-dI_p{}^{com}/dt)$. On the other hand, after pellet injection, $\tau_{Ip\text{-}decay}$ becomes shorter than the command value by a factor of ~2 for the 2nd and 3rd pellet, e.g., ~1.5 s at t~12.39 s and t~12.58 s.

The τ_{fric} calculated for W_r = 20 MeV and Z_{eff} = 3 is about 3 s, which is a value similar to that of $\tau_{Ip\text{-}decay}{}^{com}$ until t~12.76 s. If the frictional drag force is the main mechanism of the slowing down, and it determines the decay of the runaway plasma current, little loop voltage would be required to keep the current when $\tau_{Ip\text{-}decay} \sim \tau_{Ip\text{-}decay}{}^{com}$. However, a V_{loop} of several Volts is supplied in the experiment to keep I_p close to $I_p{}^{com}$ even when $\tau_{Ip\text{-}decay} \sim \tau_{Ip\text{-}decay}{}^{com}$, as seen in Fig.7. Such a V_{loop} could result in avalanche generation of runaway electrons with a time constant τ_s of < ~0.8 s after t = 12.42 s, as shown in Fig.7. The value of $E/E_c{}^A$ is ~4.5 at t = 12.42 s and ~5.7 at t = 12.54 s. Since we require a rather low W_r of ~5 MeV to obtain a τ_{fric} comparable to τ_s of ~0.8 s in order to derive $\tau_{Ip\text{-}decay}$, the presence of another mechanism is suggested for the current decay.

As a candidate mechanism to explain the current decay, we apply the Andersson-Helander model with a combined effect of pitch angle scattering and radiation reaction [28,29]. In addition to the frictional drag, this model takes account of the fact that the pitch angle of a runaway electron to a magnetic

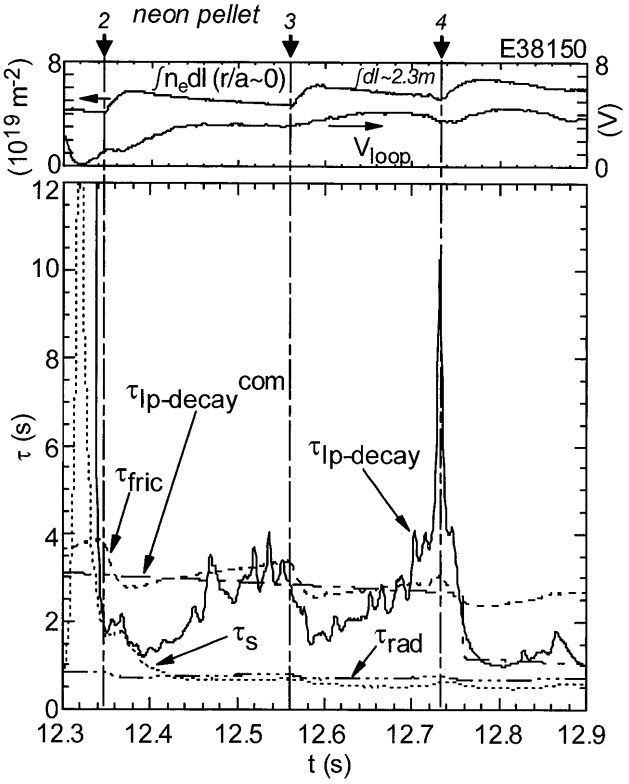

Fig. 7 Behavior of the characteristic time scales in the post-disruption runaway plasma with the impurity pellet injection. $\tau_{Ip\text{-}decay}$: decay time of plasma current defined by $I_p/(-dI_p/dt)$, $\tau_{Ip\text{-}decay}{}^{com}$: command value of decay time of plasma current defined by $I_p{}^{com}/(-dI_p{}^{com}/dt)$, τ_s: generation time of runaway electrons by avalanche process, τ_{fric}: slowing down time of an electron by frictional drag with the bulk plasma for electron energy W_r of 20 MeV and Z_{eff} = 3, τ_{rad}: slowing down time of an electron predicted by the Andersson-Helander model, including combined effect of collisional pitch angle scattering and synchrotron radiation.

field is increased by collision with bulk plasma particles, which results in the increase in synchrotron radiation from the runaway electron. The model provides the time constant τ_{rad} and the relationship between τ_{rad} and τ_{fric} as

$$\tau_{fric}/\tau_{rad} = 3.2B_t/\{(1+Z)n_e\}^{0.5},\ n_e \text{ in } 10^{19}\ \text{m}^{-3}. \quad (8)$$

The model was originally applied to explain the decay of a post-disruption current in the JET tokamak [28,30]. However, due to a lack of reliable measurements of n_e and Z during the post-disruption phase in JET, the analysis was made using assumed values, and thus uncertainty remained. On the other hand, the present analysis was made using both measured and estimated values of n_e and Z. The calculated τ_{rad} with $Z = Z_{eff} = 3$ and $B_t = 3.73$ T is ~0.8 s, as shown in Fig.7. This τ_{rad} is roughly comparable to τ_s. Therefore, τ_{rad} seems a counterpart of τ_s to derive $\tau_{Ip\text{-}decay}$.

Figure 8 shows comparison between $\tau_{Ip\text{-}decay}$ and the effective time constant τ_{eff}, where τ_{eff} is defined as $-1/\tau_{eff} = 1/\tau_s - 1/\tau_{rad}$. Generation of runaway electrons by the

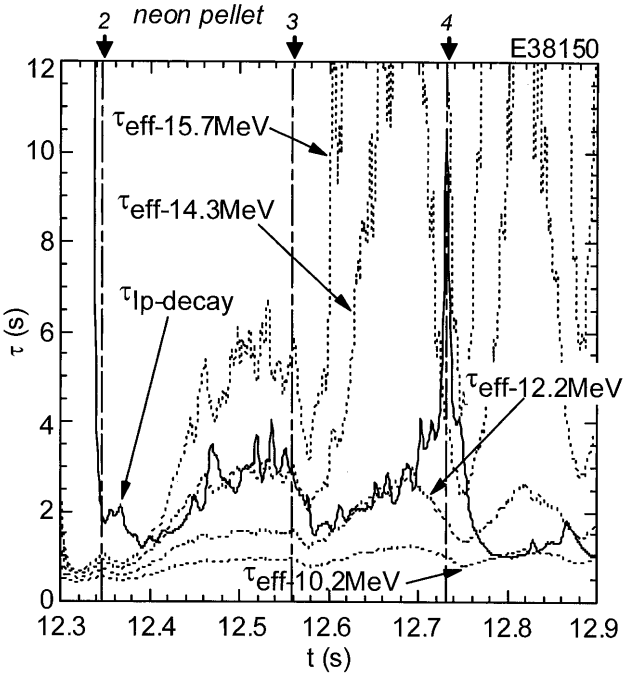

Fig. 8 Comparison between the decay time of the runaway plasma current $\tau_{Ip\text{-}decay}$ and the effective time constant τ_{eff}. The τ_{eff} is defined as $-1/\tau_{eff} = 1/\tau_s - 1/\tau_{rad}$. The τ_{eff} with different electron energy W_r is denoted as $\tau_{eff\text{-}Wr}$.

Dreicer process is neglected due to very low T_e. In Fig. 8, the $\tau_{eff\text{-}Wr}$ is calculated with different W_r, hence with different τ_{rad}. As seen in Fig.8, τ_{eff} for W_r = 14.3 MeV, $\tau_{eff\text{-}14.3MeV}$, is effectively reproduces the behavior of $\tau_{Ip\text{-}decay}$ from the beginning of the current recovery after the 2nd pellet injection, starting from t~12.4 s, to just after the 3rd pellet injection at t~12.57 s. However, $\tau_{eff\text{-}14.3MeV}$ diverges from $\tau_{Ip\text{-}decay}$ from t~12.57 s, and this is not explained by the increase in bulk electron density. Then, we introduce the reduction of W_r; i.e., τ_{eff} for W_r = 12.2 MeV, $\tau_{eff\text{-}12.2MeV}$, reproduces $\tau_{Ip\text{-}decay}$ from t~12.57 s to t~12.69 s for the 3rd pellet injection (there is a relatively large increase in $\tau_{Ip\text{-}decay}$ around t~12.71 s, but the reason for this is not clear). For the 4th pellet injection, τ_{eff} for W_r = 10.2 MeV, $\tau_{eff\text{-}10.2MeV}$, provides close value of $\tau_{Ip\text{-}decay}$ for current recovery phase.

Thus, the basic behavior of the post-disruption runaway plasma current may be due to the balance of avalanche generation and slowing down by the Andersson-Helander model with a stepwise reduction of energy of runaway electrons at the impurity pellet injection. The step of energy reduction would be approximately 2 MeV per pellet injection. In addition, these results serve to an opportunity for validation of the Andersson-Helander model.

4. Discussions

As shown in the previous section, with the impurity pellet injection, a prompt exhaust of runaway electrons was observed, and a stepwise energy reduction of runaway electrons was suggested. In order to reveal the precise dynamics of runaway electrons in the pellet and in the runaway plasma,

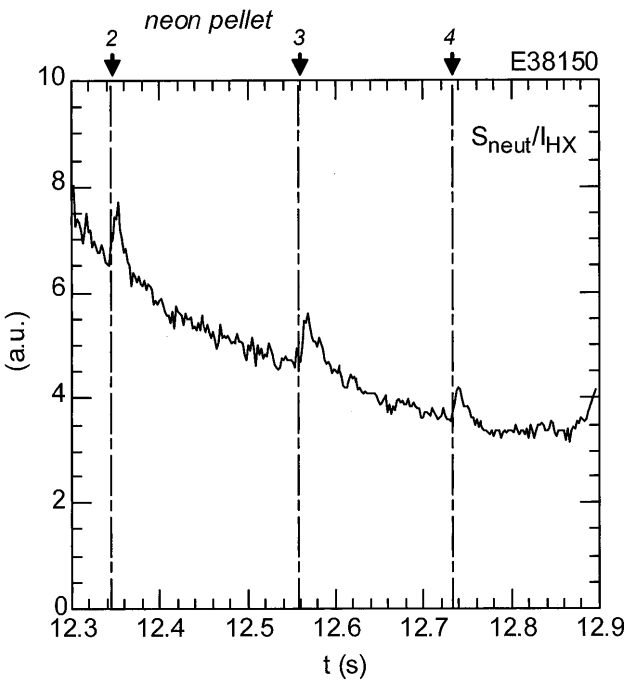

Fig. 9 Ratio of the photo-neutron emission rate S_{neut} and the hard X-ray intensity I_{HX}.

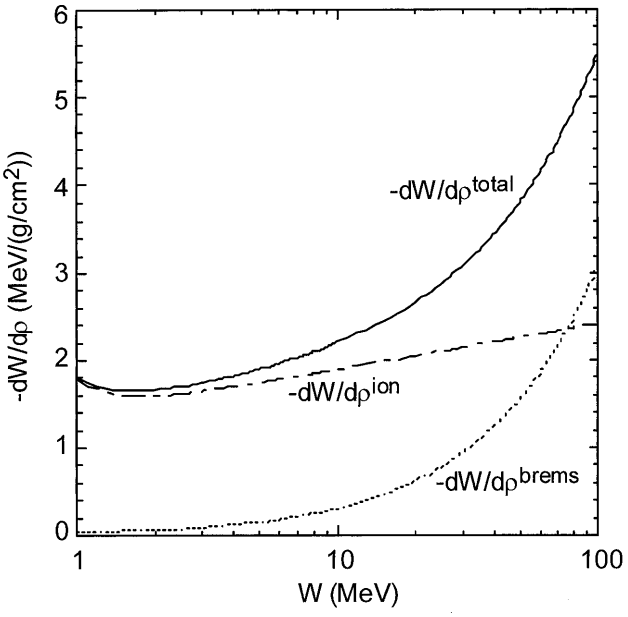

Fig. 10 Mass stopping power $-dW/d\rho$ of a relativistic electron for neon. $-dW/d\rho^{total}$: total mass stopping power defined as $-dW/d\rho^{total} = -(dW/d\rho^{ion} + dW/d\rho^{brems})$, where $dW/d\rho^{ion}$ is the stopping power by the ionization process and $dW/d\rho^{brems}$ is the stopping power by the bremsstrahlung radiation process, W is the energy of a relativistic electron.

reliable diagnostics of energy and spatial distribution, theoretical models, and simulation studies are required. Since these are beyond the scope of this paper, we will limit ourselves to discussing some of the related issues.

If the stepwise reduction of W_r shown in Sec. **3.4** actually occurs, this means not only a new property of the runaway plasma but also an additional benefit for mitigation of post-disruption runaway electrons. Unfortunately, the energy distribution of runaway electrons was not measured directly in this experiment. Instead, we used the ratio of S_{neut} to the hard X-ray intensity I_{HX}, S_{neut}/I_{HX}, as shown in Fig.9. While it is difficult to perform a precise and quantitative analysis using this ratio, the ratio is useful for discussing the change in energy distribution of lost runaway electrons. In Fig.9, S_{neut}/I_{HX} is generally decreasing in time, and this trend suggests that the energy distribution of runaway electrons is changed and the fraction of exhausted runaway electrons with higher energy becomes small. This appears to be consistent with the energy reduction indicated in Sec. **3.4**. When looking at the results in more detail, however, we note the spike-like increases in S_{neut}/I_{HX} just after the pellet injections. These increases imply that the higher-energy runaway electrons are more efficiently exhausted by pellet injections.

As we note in Sec. **3.3**, the exhaust effect of runway electrons by the pellet injection becomes smaller with the latter injections, and for the 5th to 7th pellet injections, there is no obvious plasma response, as seen in Fig.2. In this figure, the pellet size measurement (before injection to plasma) indicated that the 5th pellet was broken and the size of the 6th pellet was smaller than the normal size. The pellet size of the 7th pellet was not particularly small. Though a decrease in the number of runaway electrons that corresponds to a decrease in I_p should be considered in the ablation process of injected pellets, we may expect some response in the signal of bulk electron density. Looking at the results from Sec. **3.4** suggesting W_r of ~10.2 MeV after the 4th pellet, we suspect that there is a threshold energy of runaway electrons of ~10 MeV for interaction with the impurity pellet.

Figure 10 shows the calculated mass stopping power of a relativistic electron $-dW/d\rho$ for the case of neon using the Bethe-Heitler formula [26,31], where W is the energy of a relativistic electron, and ρ the surface mass density of the target material. In Fig.10, the total mass stopping power $-dW/d\rho^{total}$ is defined as $-dW/d\rho^{total} = -(dW/d\rho^{ion} + dW/d\rho^{brems})$, where $dW/d\rho^{ion}$ is the stopping power by an ionization process and $dW/d\rho^{brems}$ is the stopping power by bremsstrahlung radiation. When we take $-dW/d\rho^{total}$~2.7 MeV/(g/cm^2) for a 20 MeV electron, a mass density of solid neon ~1.44 g/cm^3, and an interaction length of ~2 mm, a 20 MeV electron loses its energy of ~0.8 MeV during its passage through the pellet. Within the pellet, we can imagine that the electron orbit is scattered throughout the dense material. We note that the mass stopping power increases as W increases in the region where $W \geq 2$ MeV. Especially, $-dW/d\rho^{brems}$ increases rapidly where $W \geq$ ~10 MeV, e.g., $-dW/d\rho^{brems}$ roughly doubles in value from 10 MeV to 20 MeV, i.e. from 0.31 MeV/(g/cm^2) to 0.62 MeV/(g/cm^2). The ratio of the stopping power to the electron energy is not substantially changed, but even at the same pitch angle, the higher-energy electron seems to emit higher synchrotron radiation, which is increased with square of the

perpendicular momentum of the electron to the magnetic field [28]. Also, the scattering may result in an increase in the radial transport of runaway electrons in the plasma, and such a transport seems to contribute to the enhancement of the exhaust of runaway electrons.

Estimating that there are ~2.3×10^{17} runaway electrons for I_p~0.5 MA, the reduction step of electron energy by the pellet injection of ~2 MeV corresponds to a total reduction of ~4.6×10^{17} MeV. If the pellet was ablated by the runaway electrons up to the 3rd ionization state of the neon, then an energy of ~5.6×10^{16} MeV would be needed for the ~4×10^{20} neon atoms contained in a pellet, where the energies for the 2nd and the 3rd ionization for neon are 40.962 eV and 63.45 eV, respectively. As seen in Fig.10, the stopping power by the bremsstrahlung radiation is about 1/3 of that by ionization, and a bremsstrahlung radiation of ~1.9×10^{16} MeV is expected to result from this process. So, the energy required for ionization and the bremsstrahlung radiation is ~7.5×10^{16} MeV, which is only ~1/6 of ~4.6×10^{17} MeV. Again, the effects of scattering and synchrotron radiation in the pellet should be considered.

5. Summary

The experiment of impurity neon pellets injection into a post-disruption runaway plasma has been carried out to study their mitigating effects on runaway electrons. The runaway plasma was determined to be nearly equivalent to a neon plasma with Z_{eff}~3 for T_e~10 eV. The pellet ablation was attributed to the energy deposition of relativistic runaway electrons in the pellet. A high bulk electron density of n_e^{bar} ~2.9×10^{19} m^{-3} at I_p~0.42 MA was obtained with the Greenwald density factor n_e^{bar}/n^{GW} of ~2.2. The effects of prompt exhaust of runaway electrons from the plasma and reduction of runaway plasma current without large amplitude MHD activities were found. One possible explanation for the basic behavior of runaway plasma current is that it follows the balance of avalanche generation of runaway electrons and slowing down predicted by the Andersson-Helander model, including the combined effect of collisional pitch angle scattering and synchrotron radiation. It is suggested that the impurity pellet injection reduced the energy of runaway electrons in a stepwise manner such as from 14.3 MeV to 12.2 MeV and from 12.2 MeV to 10.2 MeV.

Our results thus reveal that injection of impurity pellets has mitigating effects on post-disruption runaway electrons, and should help to clarify the characteristics of runaway plasma.

Acknowledgments

The authors wish to thank H. Ichige for operating the impurity pellet injector. The authors also acknowledge Drs. M. Nagami, T. Takizuka, T. Fujita, R. Yoshino, and Y. Miura for their fruitful discussions. This work was partly supported by a Grant-in-Aid for Scientific Research from the Japan Society for the Promotion of Science (No. 16204049).

References

[1] H. Knoepfel and D.A. Spong, Nucl. Fusion **19**, 785 (1979).
[2] ITER Physics Expert Group on Disruptions, Plasma Control, and MHD, and ITER Physics Basis Editors, Nucl. Fusion **39**, 2251 (1999).
[3] P. Helander *et al.*, *8th IAEA Technical Meeting on Energetic Particles in Magnetic Confinement Systems*, San Diego, 6-8 October 2003 (2003).
[4] G. Maddaluno *et al.*, J. Nucl. Matter. **313-316**, 651 (2003).
[5] M. Sugihara *et al.*, *20th IAEA Fusion Energy Conference*, IT/P3-29 (2004).
[6] R. Yoshino *et al.*, Plas. Phys. Control. Fusion **39**, 313 (1997).
[7] Y. Kawano *et al.*, Proc. 16th IAEA Fusion Energy Conference, Vol.1, Vienna, 345 (1997).
[8] Y. Kawano *et al.*, Fusion Sci. Tech. **42**, 298 (2002).
[9] M. Bakhtiari *et al.*, Nucl. Fusion **42**, 1197 (2002).
[10] M. Bakhtiari *et al.*, *20th IAEA Fusion Energy Conference*, EX/10-6Rb (2004), also M. Bakhtiari *et al.*, Nucl. Fusion **45**, 318 (2005).
[11] D.G. Whyte *et al.*, Phys. Rev. Lett. **89**, 055001 (2002).
[12] R. Yoshino *et al.*, Nucl. Fusion **39**, 151 (1999).
[13] Y. Neyatani *et al.*, Nucl. Fusion **39**, 559 (1999).
[14] R. Yoshino and S. Tokuda, Nucl. Fusion **40**, 1293 (2000).
[15] H. Tamai *et al.*, Nucl. Fusion **42**, 290 (2002).
[16] S. Tokuda *et al.*, Nucl. Fusion **39**, 1123 (1999).
[17] R. Jaspers *et al.*, Phys. Rev. Lett. **72**, 4093 (1994).
[18] S. Morita *et al.*, Nucl. Fusion **30**, 938 (1990).
[19] Y. Kawano *et al.*, *56th Annual Meeting of the Physical Society of Japan*, 27aXH-5 (2001).
[20] Y. Kawano *et al.*, *21st Annual Meeting of the Japan Society of Plasma Science and Nuclear Fusion Research*, 26pA01 (2004).
[21] R. Jayakumar *et al.*, Phys. Lett. **A172**, 447 (1993).
[22] R. Jaspers *et al.*, Nucl. Fusion **33**, 1775 (1993).
[23] K.H. Finken *et al.*, Nucl. Fusion **41**, 1651 (2001).
[24] T. Hatae *et al.*, Rev. Sci. Instrum. ***70***, 772 (1999).
[25] B.V. Kuteev *et al.*, Nucl. Fusion **35**, 1167 (1995), and B.V. Kuteev *et al.*, 41st Annual Meeting of the Division of Plasma Physics of the American Physical Society, FP1 86 (1999).
[26] T. Nakamura, *Radiation Physics and Accelerator Safety Engineering, 2nd Ed., Chijinshokan* (2001) (in Japanese).
[27] O.N. Jarvis *et al.*, Nucl. Fusion **28**, 1981 (1988).
[28] F. Andersson *et al.*, Phys. Plasmas **8**, 5221 (2001).
[29] P. Helander *et al.*, Plas. Phys. Contr. Fusion **44**, B247 (2002).
[30] R.D. Gill, Nucl Fusion **33**, 1613 (1993).
[31] N. Otsuka, *Q&A Houshasen Buturi, Kyouritsu Shuppan* (1995) (in Japanese).